Grid-Forming Load Planning Strategy for Stability Enhancement in Inverter Dominated Power Systems

Baity Nuris Syifa[1], Rakibuzzaman Shah[1,2], N. Mithulananthan[1], Tanazzaha Nur Izzati[3], Adlan Pradana[1], and Syed Islam[2]
[1]Department of Electrical Engineering and Computer Science, The University of Queensland, QLD 4072, Brisbane, Australia.
[2]Centre for New Energy Tranistion Research (CfNETR), Federation University Australia Mt Helen, VIC 3353, Australia.
[3]Sepuluh Nopember Institute of Technology, Surabaya 40111, Indonesia.
b.syifa@uq.edu.au, md.shah@uq.edu.au, mithulan@eecs.uq.edu.au, 5022211001@student.its.ac.id, a.pradana@uq.edu.au, s.islam@federation.edu.au

***Abstract*— The increasing penetration of inverter-based resources (IBRs) has degraded the frequency and voltage stability margin of the power system. This paper proposes a planning strategy for the Grid Forming Loads (i.e., flexible loads interfaced with Grid-Forming Inverters) in low-inertia power systems. The planning strategy includes the identification of the most suitable location and the control needed to enhance stability. The location is identified via an index known as the flexible load location index (FLLI). The FLLI integrates the synchronizing power coefficient (SPC) and inertia distribution index (IDI) to assess each bus electrical proximity to the location of disturbance and inertial contribution. The proposed strategy is validated using a modified IEEE 39 bus system with 70% large-scale PV (LSPV) penetration. The findings demonstrate that strategic GFM control placement enhances both frequency and voltage stability margin and ensures the seamless integration and operation of LSPVs.**

***Index Terms*-- Electric vehicle, frequency stability, grid forming control, inverter-based resources, voltage stability.**

I. Introduction

To meet the global clean energy and low-carbon goals, many power systems are rapidly moving toward inverter-based system design. In recent years, there has been a large increase in the use of IBRs such as solar photovoltaic (PV), wind turbine generation, and battery energy storage systems [1]. However, the rapid replacement of synchronous machines has weakened the system's ability to maintain stable frequency and voltage [2]. As a result, power systems dominated by grid-following (GFL) converters become more vulnerable to instability during disturbances [3].

Therefore, recent studies in [4],[5] have highlighted the importance of GFM control in generation sources to maintain the stability of the inverter-dominated power systems. The placement of GFM control is a crucial factor that affects its overall effectiveness. This means that the stability of the system depends not only on the total available inertia but also on how that inertia is spatially distributed and how frequency support strength is allocated across the network [5]. Uneven deployment of GFM control may jeopardize the stability margin instead of improving. This is particularly true under the weak grid condition.

Until today, GFM control only employed in various generation sources, including solar PV, wind turbine generation, and battery energy storage systems [5]. Solar PV units can operate slightly below their maximum power point to reserve headroom for voltage and frequency support, while BESS offers fast active and reactive power response through converter control [6].

However, as power systems continue to evolve, many loads are now connected to the grid through power electronic converters, such as diode rectifiers or voltage source converters (VSCs) [7]. At present, most of these loads operate in grid-following (GFL) mode. To fully utilize the demand side flexibility, these loads can be operated in grid-forming (GFM) mode, allowing them to behave as flexible voltage sources rather than current sources [8]. In GFM, P–f and Q–V droop control generate the voltage magnitude/angle and produce the instantaneous power reference P^*(and Q^*) for the unit. The grid-side converter enforces the formed AC voltage/frequency, while the DC (load-side) converter adjusts DC voltage and current so that the load sees the required DC setpoint and the actual power equal to the reference. Among various types of flexible loads, electric vehicles are particularly promising due to their large charging and discharging capacities, which allow their charging power to be rapidly adjusted in response to system conditions. Since EVs are typically connected for several hours and do not require immediate full charge, their demand can be flexibly increased or reduced during disturbances without affecting user requirements. The flexibility of GFM control in such flexible loads allows the system to maintain stability while ensuring that all PV units operate at their maximum power even during disturbance [8]. This approach eliminates the need for a headroom in solar PV units to support the grid after a disturbance.

Similar to GFM-based generation units, selecting the right buses to place GFM on EV charger loads is crucial to maintain system stability during disturbances. Thus, to make EV charger loads more useful and to strengthen their role in maintaining system stability, this paper provides two main contributions:

1) This paper introduces a flexible load location index (FLLI) to identify the best locations for placing GFM on EVCL. The index combines the Synchronizing Power Coefficient (SPC) and the Inertia Distribution Index (IDI) to show the capability of each EVCL bus in supporting GFM operation.
2) The proposed FLLI is tested under different operating conditions and disturbance scenarios to demonstrate its

979-8-3315-8138-1

effectiveness in identifying the most beneficial locations on GFM control in EVCL.

II. METHODOLOGY

A. Flexible Load Location Index (FLLI)

The objective of the proposed method is to identify the optimal location for integrating GFM control into electric vehicle charger load (EVCL). The main idea behind the FFLI index is explained next.

Starting with the conventional swing equation in (1), the frequency dynamics follow the simplified relation:

$$\frac{df}{dt} = \frac{f_0}{2H}\,\Delta P_{imb} \tag{1}$$

In (1), it shows that lower inertia (H) leads to a higher rate of change of frequency (RoCoF) $\left({df}/{dt}\right)$. Over a short interval (t), the frequency deviation at a bus (Δf_i) can be approximated by (2):

$$\Delta f_i = RoCoF_i \cdot t \tag{2}$$

The GFM droop controller responds to this frequency deviation through *P-f* droop control, and can be as expressed in (3):

$$\Delta P_{imb} = \Delta P_{ref} = \frac{1}{R}\,\Delta f_i \tag{3}$$

In (3), ΔP_{ref} is active power reference changes and R is droop gain control.

Power reference in (3) generated based on the size of power imbalance (ΔP_{imb}) that distributed through the network which depends on the synchronizing power coefficient (K_{iv}) as explained in (4):

$$\Delta P_{imb} = K_{iv}\,\Delta\delta_{iv} \tag{4}$$

In (4), $\Delta\delta_{iv}$ is angle deviation between the internal angle of the EVCL-GFM and bus where the disturbance occurs.

Assuming the delivered and commanded power are balanced at t after disturbance,

$$K_{iu}\,\Delta\delta_{iu} = {1}/{R}\,\Delta f_i \tag{5}$$

$$\Delta\delta_{iu} = \frac{1}{K_{iu}\,R}\,\Delta f_i \tag{6}$$

Substituting (1) and (2) yields,

$$\Delta\delta_{iv}(t) = \frac{1}{K_{iu}\,R_p}\left(\frac{f_0}{2H}\Delta P_{imb}\right)\cdot t \tag{7}$$

By combining (1)– (6), the relation in (7) links the droop coefficient, inertia, SPC, and internal angle deviation of the GFM unit. This shows that, for a given droop setting, the required internal angle shift to deliver a certain active-power response is mainly influenced by:

1) Synchronzing power coefficient (SPC), and
2) Spatial inertia in each bus represented by the inertia distribution index (IDI).

When the inertia in an area is low (i.e., the bus is electrically far from the center of inertia (COI) and the SPC is small, the GFM unit must undergo a larger internal angle shift to achieve the same stabilizing effect as when the EVCL operates in GFM mode at a bus with high SPC and IDI. Conversely, when GFM control is implemented in the EVCL at a bus with strong inertia support and large SPC, only a small angle adjustment is required to provide an effective stabilizing response. This condition is more desirable, as limiting the required angle deviation is crucial to ensure robust GFM operation; the internal angle of GFM converters is highly sensitive, and excessive deviations may trigger unstable behaviour.

Therefore, the proposed index can be expressed in (8):

$$FLLI(i) = K_{norm}(i)(IDI_i) \tag{8}$$

higher FLLI indicates a more suitable location for equipping GFM control in EVCL, as both $K_{\text{norm}}(i)$and IDI_ineed to be large simultaneously. If either of them is small, it will reduce the overall index value.

The SPC can be calculated using coefficient (K_{ij}) which expressed as in (9):

$$K_{ij} = \left.\frac{\partial P_{e,i}}{\partial\delta_{ij}}\right|_{\delta_{iv0}} = E_i V_j (B_{ij}\cos\delta_{ij0} - G_{ij}\sin\delta_{ij0}) \tag{9}$$

where E_i and V_j represents the internal voltage of EVCL-GFM and bus voltage respectively, δ_{ij} is the angle between E_i and V_j, G_{ij} and B_{ij} are real and reactive part of off-diagonal of bus admittance matrix (Y_{Bus}).

The K_{iv} of each EVCL based GFM can be then normalized with respect to the highest K_{iv} (10):

$$K_{norm}(i) = {K_{iv}}/{\max\,(K_{jv})} \tag{10}$$

where δ_{ij0} represents δ_{ij} during steady state conditions. From (9) the total power mismatch is distributed among all EVCL based GFM according to the SPC values, which also depends on the disturbance location.

Meanwhile, the share of inertia variation of any bus in the system D_i can be estimated as in (11):

$$D_i = \int_{t_0}^{T+t_0} (f_i(t) - f_{COI}(t))^2 dt \tag{11}$$

The distance (D_i) from the COI to the monitored Bus i can be measured over the timeframe (T) by comparing the frequency of EVCL Bus i (f_i) with f_{COI} at time $t > t_0$.

The D_i for the bus of interest can be then normalized with respect to the highest distance from the (COI) using (12):

$$IDI_i = 1 - \left({D_i}/{\max(D_j)}\right) \qquad \forall j \in \{1,..,M\} \tag{12}$$

979-8-3315-8138-1

High IDI_i values mean a relatively large electrical distance from a particular bus i to the COI. This also suggests a low inertia distribution on bus i compared to other buses.

B. Implementation Procedure

The detailed steps followed in this paper are given below:

1) Apply GFM control to each EVCL one at a time to collect all parameters required for the FLLI calculation.
2) All parameters from (8)-(12) for the FLLI calculation are obtained from the simulations and processed in Python.
3) Compute the FLLI and rank all EVCL buses to identify the most promising locations for GFM placement.
4) Activate the GFM on the highest-ranked bus and assess the system under the maximum disturbance defined in Table I. Evaluate whether whether post-disturbance voltage oscillations are reduced and settled quickly.
5) Check whether all LSPV units are still operating at their maximum power. If their power decreases or does not recover after the disturbance, this indicates that the stabilizing contribution from the selected GFM on EVCL is insufficient. Since the EV charger load capacity cannot be increased like a battery or generator, an additional EVCL-GFM must be activated based on the rank detailed in Table II.
6) Repeat steps 4 and 5 for the remaining ranked EVCL-GFM candidates until the requirement is fulfilled.

III. Case Studies and Simulation Results

Modified IEEE 39 bus system has been used for this study. Fig. 1 shows a modified IEEE 39 bus system. In this study, 70% of the total generation capacity from SGs is replaced with eight large-scale PV (LSPV) systems.

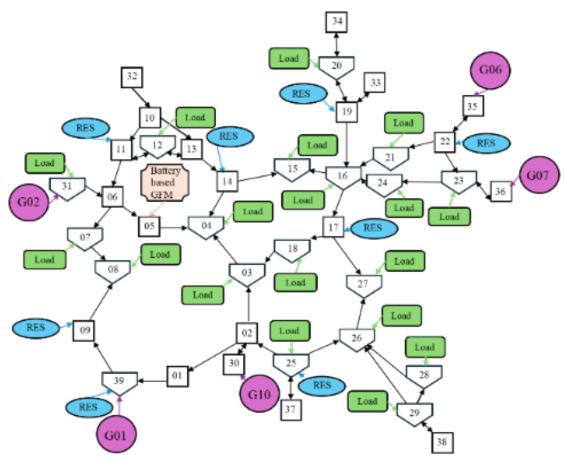

Fig. 1. Modified IEEE 39 bus test system.

The WECC model of LSPV is utilized for this study. The synchronous generators at Buses 03, 04, 05, 08, and 09 have been replaced with LSPV farms, each consisting of 54 units and providing a total generation capacity of 270 MW per farm. Additionally, five parallel battery energy storage systems (BESS) with Grid Forming (GFM) control have been installed at Bus 05, following AEMO guidelines [9]. For the simulations, a GFM battery rating of 600 MW has been selected, using the Waratah Super Battery in New South Wales, which has a capacity of 850 MW and 1,680 MWh, as a practical reference [9].

The following operating conditions as given in Table I are used for the simulation studies.

TABLE I. Different Operating Scenarios

Scenarios	**Scenario 1:** System contains of fixed PQ loads alongside the EVCLs. A generation outage (SG 06 = 650 MW, 400 MVAr) occurs at Bus 35 at t = 2 s. **Scenario 2:** The system consists of a voltage and frequency-dependent load. The system consists of 50% ZIP load (i.e., 20% constant impedance, 40% constant current and 40% constant power). The remaining load type is EVCL. Additional load **(650 MW, 400 MVAr) added on Bus 06 at t = 2 s.**

A. Scenario 1-SG 06 Outage on Bus 35 at t = 2 s

In Scenario 1, SG 06 is disconnected at Bus 35 at t = 2 s. This event represents the most severe disturbance in the study for scenario 1. The system experiences the lowest frequency, i.e., 0.96 pu at 101.9 s. The index is evaluated based on the system's response to this outage.

Based on Table II, this scenario will analyze the system response when GFM is equipped at EVCL with the highest rank (EVCL 08) and lowest rank (EVCL 28) based on FLLI. Fig. 2 shows the bus ranking based on the proposed index.

TABLE II. Bus Ranking Based on FLLI Index

EVCL	K_{norm}	1-IDI	FLLI	Rank
03	0.3005	0.576776	0.173321179	3
04	0.6433	0.854065	0.549419935	2
08	1.0000	0.990000	0.990000000	1
15	0.2624	0.339712	0.089140547	4
18	0.2462	0.317286	0.078115799	5
21	0.1757	0.185908	0.032664045	8
24	0.1984	0.166277	0.032989345	6
26	0.1560	0.172039	0.026838102	7
28	0.0681	0.000000	0.000000000	9
28	0.0681	0.000000	0.000000000	9

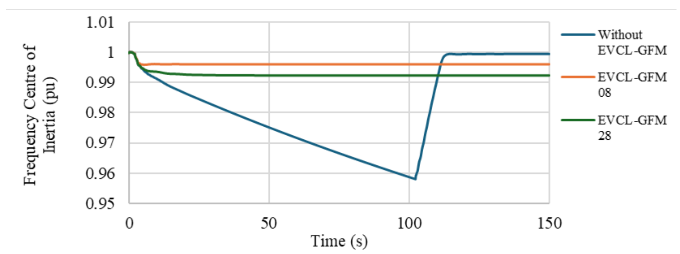

Fig. 2. Frequency COI for baseline and EVCL based GFM.

The results in Fig. 2 present the frequency COI responses for three cases: without GFM control, with GFM control on Bus 08, and with GFM control on Bus 28. Without GFM, the system experiences a deep frequency nadir of 0.9579 pu with a high RoCoF of 0.032 pu/s and a long settling time of 113.6 s, indicating a poor stability margin. When GFM control is applied at Bus 08, the frequency nadir improves to 0.9959 pu with a lower RoCoF of 0.0287 pu/s and a fast-settling time of 6.6 s. In contrast, GFM placement at Bus 28 results in a moderate improvement with a nadir of 0.9924 pu and a settling time of 28.3 s. These results confirm that the proposed FLLI accurately identifies the most effective location for equipping GFM control on EVCL.

979-8-3315-8138-1

Fig. 3 shows the voltage response across all buses following the outage of SG 06 at t = 2 s without any GFM support on EVCL. The system experiences an average voltage dip of 5.7%, and the voltage magnitudes of three buses (20, 30, and 38) fall below 0.95 pu. The voltage does not fully recover to 0.95 pu within the simulation window. Such undervoltage conditions increase current demand, risk of overheating, and trigger the protection scheme. As reflected in Fig. 3, while the frequency COI reached its lower limit (at t = 101.9 s), several PVs are tripped as well as EVCLs, resulting in further frequency and voltage collapse.

Fig. 4 shows the case where the EVCL at Bus 08 operates in GFM mode. The converter adjusts its voltage magnitude and phase through droop control. During the voltage sag, the reactive droop control injects reactive power to compensate for the loss caused by the SG06 outage, while the *P–f* droop control temporarily reduces active power consumption to relieve the power deficit. As a result, the average voltage dip is reduced from 5.7% to 3.8%, and no buses violate the 0.95 pu limit. Full recovery within the 0.95–1.05 pu range is achieved by 2.99 s. This improvement occurs because Bus 08 (the highest-ranked bus based on FLLI) is electrically well coupled to the weak area. Acting as a nearby voltage source that supplies immediate reactive power support and modulates its phase angle to resynchronize neighboring buses, resulting in faster frequency COI recovery and remarkable voltage responses (in Fig. 4).

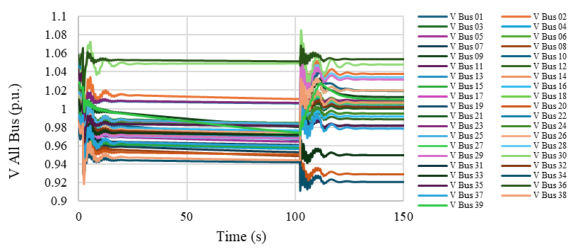

Fig. 3. Voltage profile with no GFM on EVCL.

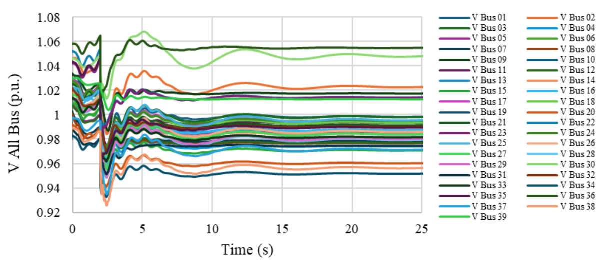

Fig. 4. Voltage profile following EVCL-GFM activation at Bus 08.

When the GFM is placed at EVCL 28, its contribution becomes noticeably weaker. As shown in Fig. 5, the average voltage dip is reduced only to 4.9%, which is better than the baseline but worse than EVCL-GFM at Bus 08.Furthermore, the recovery time extends to 3.11 s. Bus 28 has low SPC and low IDI which means the location is far from center of inertia, as reflected in its low FLLI ranking. According to (7), this condition requires a larger internal angle shift from the GFM unit to deliver the same active power support as EVCL-GFM at Bus 08. Therefore, the stabilizing power from EVCL-GFM 28 must propagate through longer transmission paths to the disturbance location (Bus 35). This increases the transfer impedance and slows the response in supporting the weak buses caused by the outage of SG 06. As shown in Fig. 2 and Fig. 5, the COI frequency is much lower than the COI frequency following the activation of EVCL-GFM 08. Moreover, post-disturbance sustained voltage oscillations confirm that GFM is located at an electrically distant site and far from the COI. It means that low-rank FLLI buses are less effective and can stress the converter due to larger angle shifts.

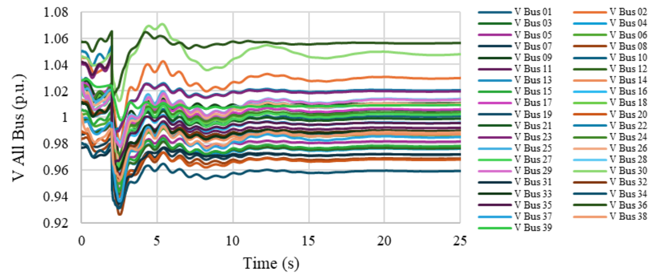

Fig. 5. Voltage profile following EVCL-GFM at Bus 28.

It is also important to note that Figs. 6 and 7 show different steady-state power consumption levels for EVCL at Buses 8 and 28. However, the results from scenario 2 (in the next section) confirm that the dominant factor is not the EVCL consumption itself, but rather the quality of the EVCL bus location, which enables the GFM to support system voltage and frequency stability effectively.

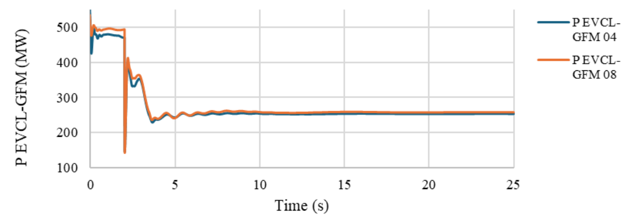

Fig. 6. EVCL-GFM active power comparison (Bus 08 vs Bus 28).

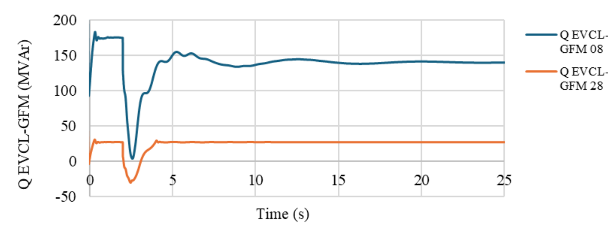

Fig. 7. EVCL-GFM reactive power comparison (Bus 08 vs Bus 28).

B. Scenario 2-Additional Load on Bus 06 at t = 2 s

In scenario 2, instead of PQ load, the voltage and frequency dependent load (VFDL) has been considered. Thus, the frequency COI is recalculated to consider contribution from VFDL on inertial response. The inertia from each of VFDL (H_{VFDL}) can be calculated using (13):

$$H_{VFDL} = \frac{\Delta P_{VFDL}(t)}{2 * {df(t)}/{dt}} \tag{13}$$

In (13), $\Delta P_{vfdl}(t)$ is VFDL changes power consumption that can be calculated using RV method detailed in [10], ${df(t)}/{dt}$ RoCoF of each VFDL bus.

The corresponding inertia estimates for all VFDL buses are summarized in Table III.

979-8-3315-8138-1

TABLE III. ESTIMATED VFDL INERTIA

VFDL Bus	07	12	16	20	23	25	27	29	31
Inertia (s)	1.53	0.05	3.35	6.73	2.19	1.41	1.96	2.56	0.11

Fig. 8 and Fig. 9 show that the reduction in power consumption at Bus 04 is significantly greater than that at Bus 08.

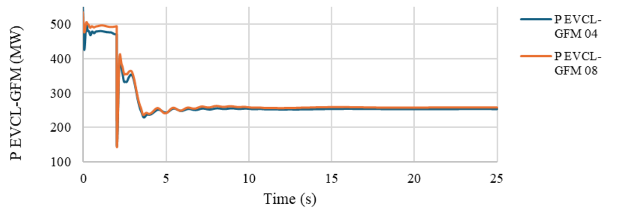

Fig. 8. EVCL-GFM active power comparison (Bus 04 vs Bus 08).

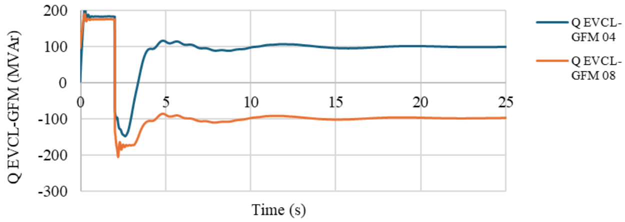

Fig. 9. EVCL-GFM reactive power comparison (Bus 04 vs Bus 08).

Although the EVCLs at Buses 04 and 08 have similar power consumption under normal conditions, their effectiveness as GFM load is different. When GFM control is applied at Bus 08, the load provides a stronger stabilizing contribution, which reduces the reactive power injection required from the LSPVs to maintain stability of the system and allows them to remain at their maximum power output, as shown in Fig. 10. In contrast, GFM operation on EVCL at Bus 04 (Fig. 11) leads to higher reactive power support being supplied by the LSPVs, forcing them to keep headroom and preventing operation at maximum power.

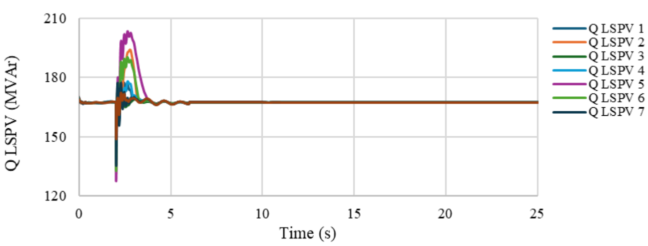

Fig. 10. LSPV reactive power following EVCL-GFM activation at Bus 08.

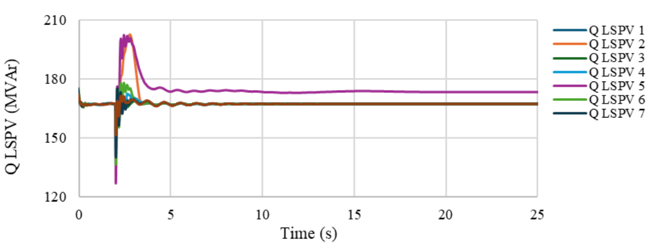

Fig. 11. LSPV reactive power following EVCL-GFM activation at Bus 04.

This difference is consistent with the rank proposed by FLLI in Table II. GFM-EVCL on Bus 08, with higher SPC and near COI, provides more effective voltage and frequency support than Bus 04, despite similar EVCL consumption during steady-state.

IV. CONCLUSIONS

This paper proposed a flexible load location index (FLLI) to identify the optimal location for grid-forming (GFM) control on EVCL. By combining the synchronizing power coefficient (SPC) and inertia distribution index (IDI), the FLLI ranks buses based on electrical coupling and total inertia in the area. Simulation studies on a modified IEEE 39 bus system with 70% LSPV penetration show that applying GFM control at Bus 08 achieves the best dynamic performance, improving the frequency nadir from 0.9579 pu to 0.9959 pu. It also reduces post-disturbance voltage dips and voltage oscillations. Overall, the proposed FLLI offers a robust and interpretable framework for deploying GFM on EVCL load buses. Future work will extend this approach to real-world scenarios under varying renewable and load conditions. Moreover, it will also consider economic aspects and control coordination between all GFL and GFM controls.

ACKNOWLEDGMENT

This research is supported in part by the Australian Research Council under Grant DP230100801. The authors sincerely thank the funding body for their generous support, which enabled the successful completion of this research.

REFERENCES

[1] H. Setiadi, B. N. Syifa, M. Abdillah, and Y. Afif, “Smart virtual rotor for frequency stability enhancement considering inverter-based renewable energy sources,” *Bulletin of Electrical Engineering and Informatics*, vol. 14, no. 5, pp. 3959–3968, Oct. 2025.

[2] U. Akram, R. Shah, N. Amjady, N. Mithulananthan, and S. Islam, “Active and reactive power injection of energy storage for short-term frequency stability in islanded power systems,” *Journal of Energy Storage*, vol. 90, p. 111914, May 2024.

[3] B. N. Syifa, N. Mithulananthan, R. Shah and J. Feng, "PMU placement to estimate power mismatch for frequency stability assessment," in *IEEE North-East India International Energy Conversion Conference and Exhibition (NE-IECCE)*, Silchar, India, 2025, pp. 1-6.

[4] B. Liao, Y. Wen and C. Y. Chung, "Minimum frequency support strength evaluation and allocation of inverter-dominated power systems," *IEEE Trans. Sustainable Energy*, vol. 99, pp. 1-12, 2025.

[5] D. A. Kez, A. M. Foley and D. J. Morrow, "Analysis of Fast Frequency Response Allocations in Power Systems With High System Non-Synchronous Penetrations," *IEEE Trans. Industry Applications*, vol. 58, no. 3, pp. 3087-3101, 2022.

[6] Z. Li, Q. Wang, Y. Luo, F. Chen, and X. Wang, “Coordinated self-tuning frequency support control strategy for wind turbine and energy storage battery against time-varying operating conditions,” *Journal of Energy Storage*, vol. 139, p. 118843, Oct. 2025.

[7] Y. Li, Y. Gu and T. C. Green, "Revisiting grid-Forming and grid-following inverters: A duality theory," *IEEE Trans. Power Systems*, vol. 37, no. 6, pp. 4541-4554, Nov. 2022.

[8] O. Gomis-Bellmunt, S. D. Tavakoli, V. A. Lacerda and E. Prieto-Araujo, "Grid-forming loads: Can the loads be in charge of forming the grid in modern power systems?," *IEEE Trans Smart Grid*, vol. 14, no. 2, pp. 1042-1055, Mar 2023.

[9] Australian Energy Market Operator, *Quarterly Energy Dynamics Q2 2025*, Melbourne, Australia: AEMO, Jul. 2025.

[10] D. Zografos, M. Ghandhari, and R. Eriksson, “Power system inertia estimation: Utilization of frequency and voltage response after a disturbance,” *Electric Power Systems Research*, vol. 161, pp. 52–60, Aug. 2018.

979-8-3315-8138-1